Contents lists available at ScienceDirect

Chemical Engineering Research and Design

journal homepage: www.elsevier.com/locate/cherd

Structural investigation of phosphonium-based ionic liquid impregnated mesostructured silica nanoparticles and application towards the adsorption of Pb(II)

Mochamad L. Firmansyah[a,*], *Nurul S. Hassan*[b], *Aishah A. Jalil*[b,c], *Rino R. Mukti*[d,e,f], *Lee Peng Teh*[g], *Herma D. Setiabudi*[h,i]

[a] *Nanotechnology Engineering, Faculty of Advanced Technology and Multidiscipline, Airlangga University, Jl. Dr. Ir. H. Soekarno, Surabaya 60115, Indonesia*

[b] *School of Chemical and Energy Engineering Engineering, Faculty of Engineering, Universiti Teknologi Malaysia, UTM Johor Bahru, 81310, Johor, Malaysia*

[c] *Centre of Hydrogen Energy, Institute of Future Energy, UTM Johor Bahru, 81310 Johor, Malaysia*

[d] *Division of Inorganic and Physical Chemistry, Faculty of Mathematics and Natural Science, Institut Teknologi Bandung, Jl. Ganesha 10, Bandung 40132, Indonesia*

[e] *Research Center for Nanoscience and Nanotechnology, Institut Teknologi Bandung, Jl. Ganesha 10, Bandung 40132, Indonesia*

[f] *Research and Innovation Center for Advanced Materials, Institut Teknologi Sumatera, Jl. Terusan Ryacudu, Lampung 35365, Indonesia*

[g] *Department of Chemical Sciences, Faculty of Science and Technology, Universiti Kebangsaan Malaysia, UKM Bangi, 43600, Selangor, Malaysia*

[h] *Faculty of Chemical and Process Engineering Technology, College of Engineering Technology, Universiti Malaysia Pahang, Lebuhraya Tun Razak, Gambang, Kuantan, Pahang, 26300, Malaysia*

[i] *Centre of Excellence for Advanced Research in Fluid Flow, Universiti Malaysia Pahang, Gambang, Kuantan, Pahang, 26300, Malaysia*

ARTICLE INFO

Article history:
Received 5 August 2021
Received in revised form 21 November 2021
Accepted 15 December 2021
Available online 22 December 2021

Keywords:
Water pollution
Ionic liquid
Adsorption
Mesostructured silica nanoparticles
Lead

ABSTRACT

Adsorption has been widely used in waste water treatment due to its simplicity and cost-effective process. One of the popular adsorbent was silica due to their advantageous properties. Immobilizing additive onto particular adsorbent is one of the way to enhance adsorption capacity. Immobilizing ionic liquid (IL) onto silica-based support could alleviate the drawbacks of IL and enhance the adsorption capacity. Thus, silica-based materials, silica and mesostructured silica nanoparticle (MSN), were impregnated with a phosphonium-based ionic liquid (IL), trioctyldodecylphosphonium bromide ($P_{8,8,8,12}Br$), which was designated as IL@SIL and IL@MSN. The structural variation of the support greatly impact the adsorbent performance. The results showed that IL@MSN with superior surface properties exhibit a faster reaction kinetic and lower thermodynamic barrier for the adsorption of Pb(II). Both adsorbents followed a pseudo second-order kinetic and chemically adsorbed Pb(II). IL@MSN showed a higher adsorption capacity in both batch and column adsorption than that of IL@SIL. The equilibrium data of both adsorbents fitted well with the Freundlich isotherm model with maximum adsorption capacity of 256.4 and 142.9 mg g^{-1} for IL@MSN and IL@SIL, respectively. In agreement with the batch experiment, IL@MSN showed a higher adsorption capacity in column adsorption than that of IL@SIL (325.6 and 242.2,

* *Corresponding author.*
E-mail addresses: ml.firmansyah@stmm.unair.ac.id (M.L. Firmansyah), nurulsahida@utm.my (N.S. Hassan), aishahaj@utm.my (A.A. Jalil), rino@chem.itb.ac.id (R.R. Mukti), lpteh@ukm.edu.my (L.P. Teh), herma@ump.edu.my (H.D. Setiabudi).
https://doi.org/10.1016/j.cherd.2021.12.025

respectively). Column adsorption with IL@MSN was able to achieve 94% removal of Pb(II) while IL@SIL achieved 70%. Superior surface properties of IL@MSN allowed a longer duration of column exhaustion than that of IL@SIL. The column experimental data showed a good fit with the Thomas model. Immobilized IL on silica based materials has potential as an adsorbent for heavy metals and structural variation over the support material played an important role.

1. Introduction

Heavy metals, which mainly comes from manufacturing and mining industry, possess a high risk to the environment and human health (Ali et al., 2019). Lead is one of the most widely used in industry, such as refinery and machinery manufacturing (Sankhla et al., 2019). The upper limit that was adapted by government of Indonesia for Pb(II) in the wastewater is between 0.3-1.0 mg L^{-1} (Ministry of Environment and Forestry of The Republic of Indonesia, 2014). Hence, the removal of Pb(II) ions from the water and waste water is highly paramount in terms of safety of health and environment. A wide selection of methods has been reported to remediate the water condition, such as ion exchange, nanofiltration, precipitation, selective liquid–liquid extraction, photocatalysis (Sharma et al., 2021), and adsorption (Bandehali et al., 2020; Goyal et al., 2021; Halli et al., 2020; Jumina et al., 2020). Adsorption is frequently used in water treatment mainly due to its efficiency, simplicity, and reasonable cost (Shahbazi et al., 2012). Adsorption process has been used to treat various kinds of pollutant, such as dye, metals, organic compound and carbon dioxide (Sharma et al., 2021). Silica has been widely used in metal removal and remediation owing to their advantages, such as availability, controlled surface properties and high surface area. Moreover, binding capacity and affinity can be adjusted through chemical modification (Da'na, 2017). However, heterogeneous and irregular pore size, and low capacity and affinity are main drawbacks of silica. Mesoporous silica, such as mesostructured silica nanoparticles (MSN) has been gaining interest in many field of application due to their advantageous properties, such as thermal and structural stability. Pore and structural uniformity and accessible adsorption sites provide a high potential as adsorbent for adsorption of various metals (Huynh et al., 2021; Triwahyono et al., 2019).

Ionic liquids (IL) have been utilized as extracting agent for various kind of metals in liquid-liquid extraction. However, liquid-liquid extraction of metals typically consume a large amount of either IL or organic solvents, which drastically increase their cost-of-operation and environmental impact. Moreover, the loss of IL in liquid-liquid extraction in unavoidable and could hampered IL viability for multiple use. Thus, immobilization of ILs on a solid support as solid phase extractors could minimize the cost-of-operation and environmental impact due to loss of IL and massive use of organic solvent, and it has a high chance of being reusable. Mesoporous silica was chosen as support material due to their surface properties, stability and ease of modification, albeit it is physical or chemical. Initial report on the immobilization of IL onto silica-based materials was done by Ayata et al. (2011) and Al-bishri et al. (2012).

Ayata et al. (2011) and Al-bishri et al. (2012), reported an impregnation of imidazolium-based IL onto silica powder. The support and ILs was connected through a hydrogen bond formed from the functionalized amine and the imidazolium ring. Although, report from Al-Bishri et al., put on emphasize on nano-silica, the effect of structural variation of the support, such as surface area and porosity was not thoroughly discussed. A little research has gone into exploring adsorption of heavy metals using a phosphonium-based IL. Phosphonium-based IL (PIL) has several advantageous over nitrogen-based IL, such as better thermal stability, higher hydrophobicity and the absence of acidic proton (Bradaric et al., 2003). The high hydrophobicity of PIL prevents the leakage of IL onto the aqueous solution during the adsorption process. This factor could extend the usability of an adsorbent. Initial report by Mohamed et al. (2017), in 2017 shows that trihexyltetradexyl bis(2,4,4-trimethylpentyl)phosphinate (Cyphos 104) for the removal of neodymium and gadolinium. The adsorption followed a single layer process and the regeneration of adsorbent was feasible owing to the IL stability. The removal was done through the complex formation between the metals with the anion of the IL. The synergistic effect of PIL and mesoporous silica could provide an excellent adsorbent for removal of heavy metals, such as Pb(II). For commercial application, adsorbent should be able to work for a long-period of time. However, most of these studies performed the adsorption in batch experiment, which lacks the ability to observe the adsorbent performance over long-period of time. Thus, a column adsorption could provide an insight on the adsorbent performance over a long-period of time.

Thus, herein we reported the immobilization of a phosphonium-based IL, trioctyldodecylphosphonium bromide ($P_{8,8,8,12}Br$) onto silica and mesostructured silica nanoparticles (MSN). The adsorbent were characterized by SEM, TEM, electron imaging, FTIR spectroscopy, X-ray diffraction and surface analyzer. The removal of Pb(II) was done in batch adsorption and column adsorption. The objective of the work is to find the adsorption behavior of the impregnated adsorbent, the performance of the adsorbent over long-period of time and the effect of structural variation of IL impregnated silica-based adsorbents towards the Pb(II) adsorption.

2. Material and methods

2.1. Materials

Trioctylphosphine (97%) and 1-bromododecane (97%), which were used as precursors for trioctyldodecylphosphonium bromide ($P_{8,8,8,12}Br$), were obtained from Sigma Aldrich (Tokyo, Japan) and Tokyo Chemical Industry Co., Ltd (Tokyo, Japan), respectively. Ethylenediamine tetraacetate (EDTA, 98%), Pb(II) standard solution in 0.5 mol L^{-1} HNO_3, cetyltrimethylammonium bromide, ethylene glycol, tetraethyl orthosilicate (99%), dithizoneand vanadate-molybdate reagent (99%) were purchased from Merck. Ammonium hydroxide was purchased from Qrec. NH_4OH, Silica (98%), aminopropyl triethoxysilane (99%) and dichloromethane (98%) were purchased from Sigma-Aldrich. Acetone (98%) was purchased from Himedia, India.

2.2. Preparation of $P_{8,8,8,12}Br$ impregnated silica support

Mesostructured silica nanoparticles (MSN) was synthesized following the report from Aziz et al. (2014). Initial mixture of MSN contained the cetyltrimethylammonium bromide, ethylene glycol, NH_4OH and water with mol ratio of 1:62:62:31, was stirred for 30 min. Tetraethyl orthosilicate, TEOS (0.0012 mol) and 3-aminopropyl triethoxysilane, APTES (0.001 mol) were added and the stirring was continued for 2 h. The final mixture showed a white suspension solution. The final mixture was then separated via centrifugation and the solid was washed thoroughly with deionized water. The synthesized MSN was air-dried at 383 K for overnight and calcined in a muffle furnace at 823 K for 3 h.

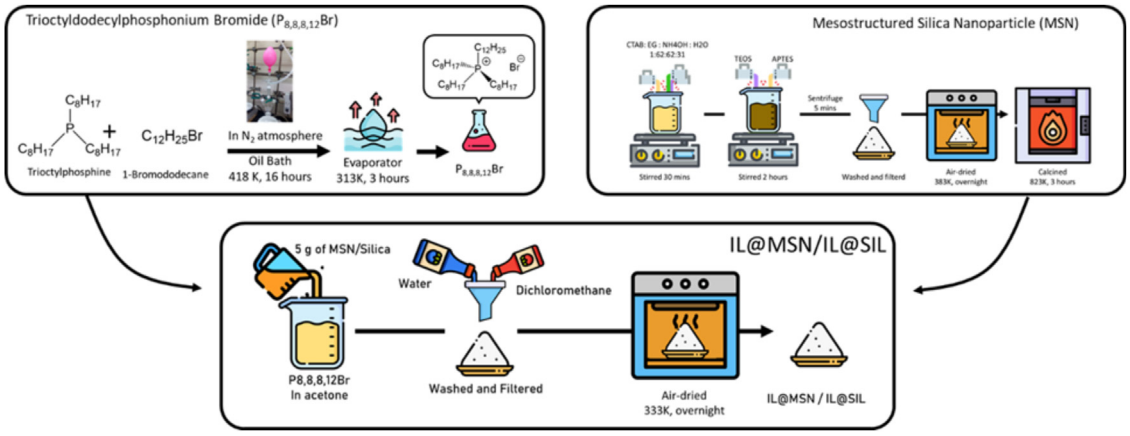

Fig. 1 – Synthesis scheme of IL@MSN.

Trioctyldodecylphosphonium bromide ($P_{8,8,8,12}Br$) in silica impregnation was prepared as described previously (Firmansyah et al., 2020). Initially, $P_{8,8,8,12}Br$ in acetone was mixed with 5 g of silica or MSN (10-50%wt. loading) and then stirred overnight. The final mixture was filtrated and extensively washed with dichloromethane and distilled water. Then, the solids were air-dried at 333 K for overnight. $P_{8,8,8,12}Br$ loaded onto silica and MSN were labeled as IL@SIL and IL@MSN, respectively. The graphical schematic of the synthesis process was shown in Fig. 1. During the adsorption process, mechanical force could dissolve the $P_{8,8,8,12}Br$ into the liquid phase. In order to determine the degree of leakage of $P_{8,8,8,12}Br$, both adsorbents were washed by water. The degree of leaking was determined through analysis of phosphorus in the washing solution by using an inductively coupled plasma – optical emission spectroscopy (ICP-OES, PlasmaQuant PQ9000 Elite, Analytik Jena GmbH). 1 g of the adsorbent was consecutively rinsed with water for 5 times; as observed the results revealed that there are no observable loss of weight and no significant presence of phosphorus in washing solution. This is due to the high hydrophobicity and low solubility of $P_{8,8,8,12}Br$ in water.

2.3. *Characterization of adsorbent*

Impregnated adsorbents were characterized by using FTIR spectroscopy, electron imaging, x-ray diffraction, and surface analyzer. The FT-IR spectra of the samples were recorded in a range of 400-4000 cm^{-1} on a Thermo Nicolet Avatar 360, Thermo Fisher Scientific Inc., USA. The morphological properties of adsorbents were performed using Scanning Electron Microscopy (SEM, Phenom Desktop ProXL, Thermo Fisher Scientific Inc., USA) and Transmission Electron Microscopy (TEM, Philips EM420, Philips, Netherland). X-ray diffraction (XRD) was recorded by using D2 Phaser X-ray diffractometer (Bruker, USA) with a scanning speed of 2° min^{-1} in a range of 2θ = 10–90°. The surface properties of the adsorbents were recorded by using Quantachrome Novatouch Lx4 (Anton-Paar GmbH, Austria). The specific surface area and pore size distribution were calculated by using BET and BJH method, respectively.

2.4. *Adsorption procedure*

2.4.1. *Batch adsorption*

Adsorption experiment was done by mixing determined amount of adsorbent with 50 mL Pb(II)-containing solution at determined temperature for a period of time. Pb(II) in the solution was determined using dithizone as complexing agent and analyzed by UV-vis spectrophotometer. Atomic absorption spectrometer (AAS, Perkin-Elmer 5100 PC, PerkinElmer Inc. USA) was used in a multi-element analysis. Adsorption efficiency and equilibrium adsorption capacity (q_{eq}) were calculated as follows,

$$E(\%) = ((C_i - C_{eq})/C_i) \times 100 \quad (1)$$

$$q_{eq} = ((C_i - C_{eq})/W) \times V \quad (2)$$

where C_i and C_{eq} are the metal concentration (mg L^{-1}) in initial and equilibrium phase, respectively. V and W are the volume of metal-containing solution and the weight of adsorbent, respectively. All experiment was performed in triplicate to obtain reliable data.

2.4.2. *Column adsorption*

Column adsorption experiment was performed in a glass column with a length 30 and 2.0 cm internal diameter. The column was packed according to Fig. 2. Glass wool which could aid as a filter aid provided at the top and bottom of the column. The adsorbent was placed from top to bottom and then covered glass beads (4 mm) to ensure the influent was distributed properly. Peristaltic pump was used to pump the influent solution at a controlled flow rate. Parameters, such as bed depth (10, 15, and 20 cm), flow rate (5, 10, 15 mL min^{-1}) and influent concentration (50, 100, 200 mg L^{-1}) were investigated. The effluent was sampled at regular intervals of ten minutes.

The value of effluent volume (V_{eff}, mL), total mass of metal adsorbed (q_{tot}, mg), maximum uptake (q_{eq}, mg), total amount of metal entering column (m_{tot}, mg) and Pb(II) removal efficiency (E,%) can be calculated from the Eqs. (3)–(7), respectively.

$$V_{eff} = Q \cdot t_{tot} \quad (3)$$

$$q_{tot} = (Q/1000) \int_{t=0}^{t=tot} \cdot C_{ad}\, dt \quad (4)$$

$$q_{eq} = (q_{tot}/m) \quad (5)$$

$$m_{tot} = (C_i \cdot Q \cdot t_{tot})/1000 \quad (6)$$

$$E(\%) = (q_{tot}/m_{tot}) \times 100 \quad (7)$$

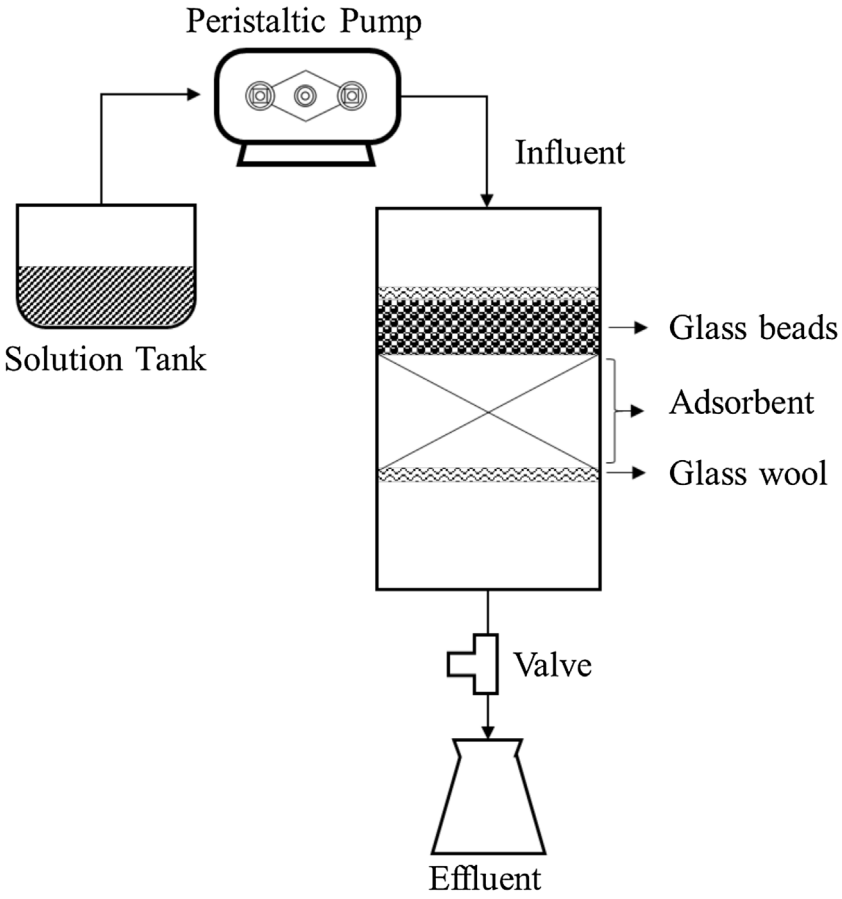

Fig. 2 – The schematic of the fixed-bed adsorption column for experimental study.

where Q is the volumetric flow rate (mL min^{-1}), t_{tot} is the total flow time (min), and C_{ad} is the concentration of metal removal (mg L^{-1}).

2.5. *Metal determination*

Spectrophotometric determination of Pb(II) was performed by dithizone as complexing agent following the approach reported by Palupi et al. (2020). Initially, a solution containing 10–100 mg L^{-1} of Pb(II) was prepared. Then, 3 mL of 60 mg L^{-1} dithizone was added to the Pb(II)-containing solution. Pb(II) – dithizone complex shows red color with absorbance peak at 500 nm. All experiments and spectrophotometric measurements were conducted in triplicate to minimize the error, which did not exceed 4%. Spectrophotometric analysis was performed with a Hinotek N4S UV-vis spectrophotometer (Ningbo Hinotek Technology Co., Ltd., China). The absorbance of the solutions was measured using 1 cm-thick quartz cell against double-distilled water as the blank, unless stated otherwise.

3. Result and discussions

3.1. *Characterization of the adsorbent*

Morphological properties and structural analysis of IL@SIL and IL@MSN was carried out by using SEM, TEM, and XRD. SEM images of the adsorbent are shown in Fig. 3a and b. IL@SIL showed a micro-granulated particles and IL@MSN showed a rough and interconnected particle. In agreement with SEM analysis, TEM of IL@MSN (Fig. 3c) also showed a porous particle with an irregular shape. In addition, elemental analysis with EDX (inset Fig. 3a and b) confirmed the presence of IL after impregnation. EDX spectra of both adsorbents show the characteristic peak of phosphorus atom that originates from the cationic center of $P_{8,8,8,12}Br$. Both adsorbents possess an amorphous nature which was reflected in the XRD patterns with the broad diffraction in the range of $2\theta = \sim 23^{\circ}$ (Nasir et al., 2020).

The N_2 physisorption profile of IL@MSN and IL@SIL was presented in Fig. 4a and b. IL@MSN and IL@SIL showed a stark different in their isotherm profile. IL@MSN exhibited a type IV isotherm, while IL@SIL showed a type II isotherm. IL@MSN possessed a type H1 hysteresis loop which associated with the presence of mesoporosity in those materials. Besides, capillary condensation at $P/P_o = 0.3$ indicated the presence of intraparticle porosity on the material (Bukhari et al., 2021). This was supported by the pore distribution from BJH method, which showed the presence of intraparticle porosity in the range of 2–4 nm, as demonstrated in Fig. 4a. On the other hand, IL@SIL showed a type H_3 hysteresis loop, which indicated the presence of random interconnected pores within the adsorbent. A small capillary condensation with gradual slope was observed in the IL@SIL isotherms, which associated with the presence of interconnected cylindrical pore in IL@SIL (Hamid et al., 2017). The presence of this interconnected pore was evidenced by wide pore distribution of IL@SIL, as shown in Fig. 4b. Due to the presence of interparticle mesoporosity, MSN showed a significantly higher surface area and pore volume than that of silica, as shown in Table 1. However, immobilization of $P_{8,8,8,12}Br$ onto MSN and silica alter their surface properties. The surface area and porosity of both adsorbents was decreased post impregnation. Silica shown a more prominent decrease in surface properties than that of MSN, especially in pore volume. This

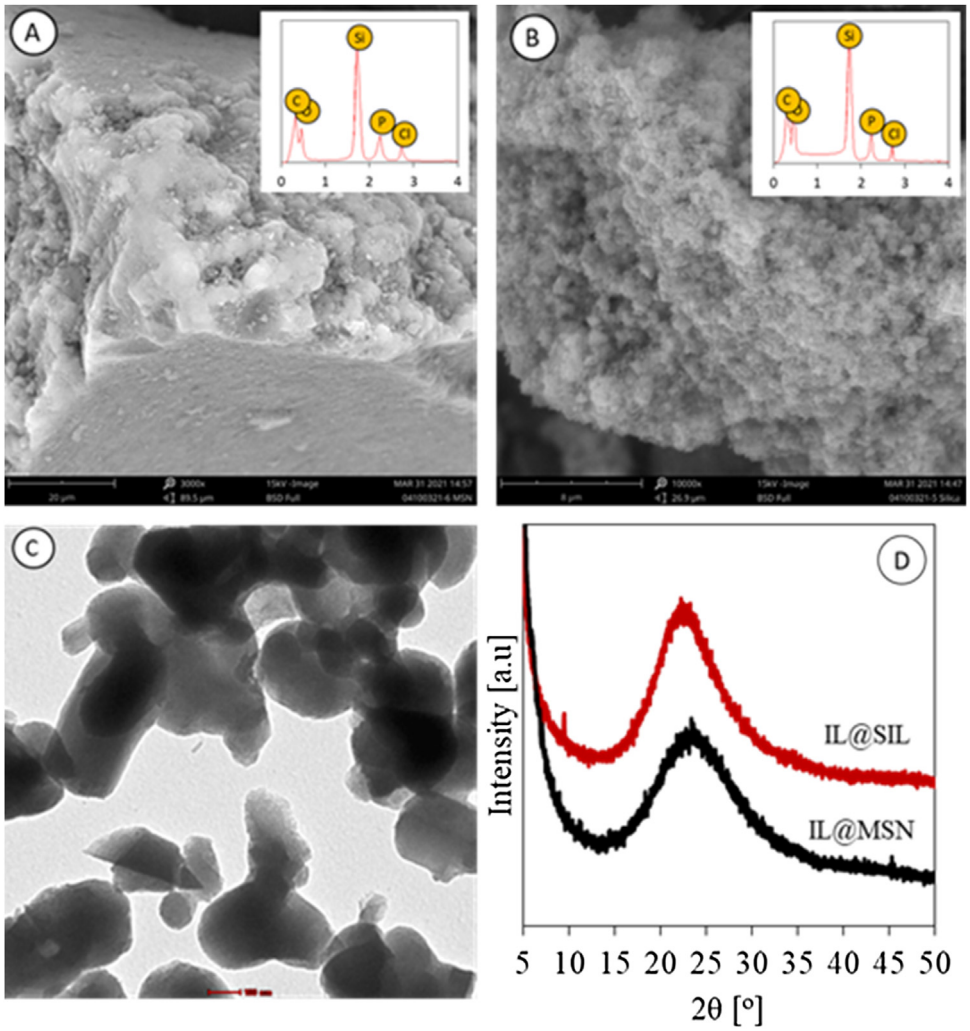

Fig. 3 – SEM images (inset: EDX spectra) of (A) IL@MSN and (B) IL@SIL, (C) TEM image of IL@MSN and (D) XRD spectrum of IL@MSN and IL@SIL.

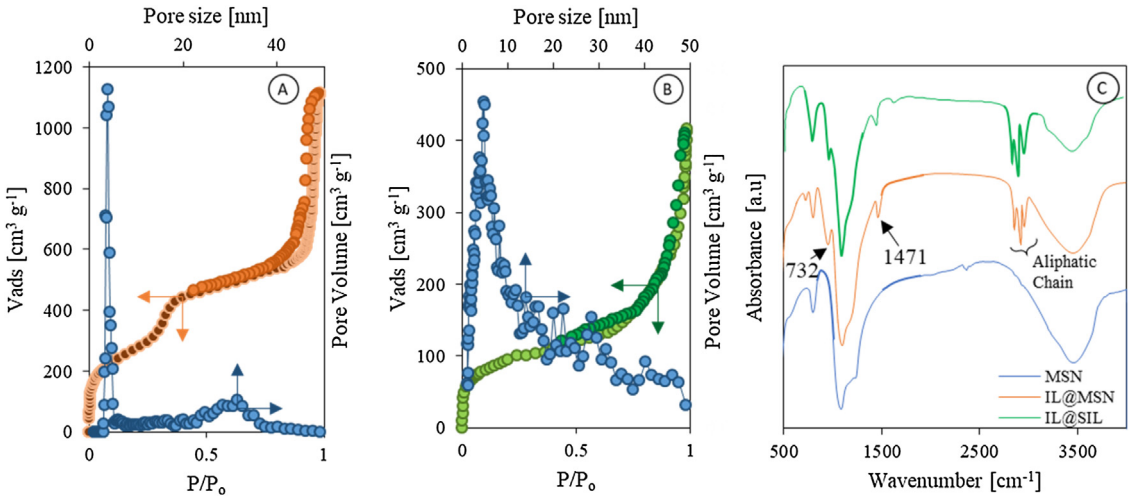

Fig. 4 – N_2 Physisorption of (A) IL@MSN and (B) IL@SIL, (C) FTIR spectrum of IL@MSN and IL@SIL.

could be associated with the pore blockage due to the presence of $P_{8,8,8,12}Br$.

The chemical signature of the adsorbents was characterized by using FTIR spectrophotometer, as shown in Fig. 4c. The spectra of MSN, IL@MSN and IL@SIL showed the presence of Si—O—Si due to the appearance of a peak between 1000–1070 cm^{-1} and between 800–810 cm^{-1}, which was associated with asymmetric stretching and symmetric stretching vibration of Si—O—Si (Rameli et al., 2018). After the impregnation process, signature peak of IL was present in the adsorbent IR spectra. New peaks at 1471 and 732 cm^{-1} were observed in the IL@SIL and IL@MSN IR spectra, which could be ascribed to the P—C deformation and stretching vibrations originating from the cationic moieties of the $P_{8,8,8,12}Br$ (Dharaskar et al., 2014). Moreover, peak from the aliphatic chain of $P_{8,8,8,12}Br$

Table 1 – Surface properties of IL@MSN and IL@SIL.

Catalyst	BET surface area [m^2 g^{-1}]	Total pore volume [cm^3 g^{-1}]
IL@MSN	1073	1.2195
MSN	1109	1.2855
IL@SIL	346	0.6936
Silica	412	0.7671

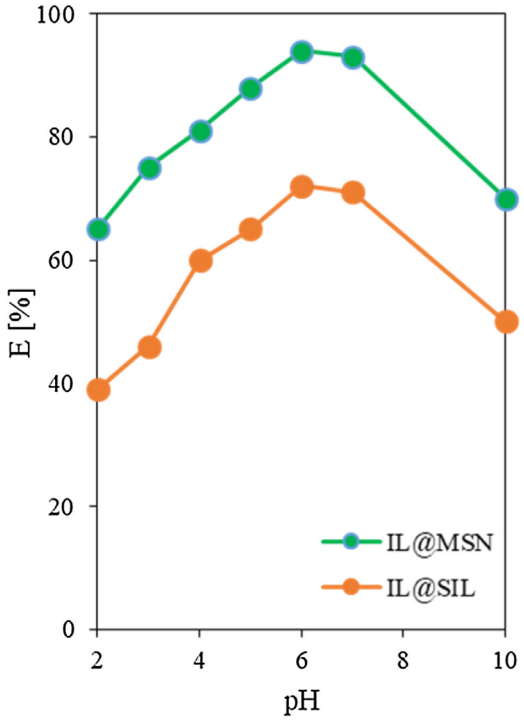

Fig. 5 – Effect of pH on the adsorption of Pb(II); [Pb(II)]: 50 mg L^{-1}, adsorbent: 1 g, $P_{8,8,8,12}Br$ loading: 50%, time: 90 min, T: 298 K.

were observed in the range of 2500–2800 cm^{-1} (Ullah et al., 2016).

3.2. *Effect of pH*

The pH of the system influences the charge density of the adsorbent as well as the complex form of Pb(II) ions in the solutions. Thus, pH holds important role in determining the adsorption performance of a system. Fig. 5 shows the effect of pH on the adsorption of Pb(II) ions. The plot shows the removal of Pb(II) increased with increasing of pH from 2 to 7. Then, the efficiency was plateau at pH of 7–8 followed by a decrease in pH higher than 9. Point of zero charge (pH_{pzc}) of both adsorbent was determined by pH drift methods, as reported by Sharma et al. (2020). Following the result, pH_{pzc} of both adsorbent was found to be 7. Thus, the surface of the adsorbent was positively charge below that point and negatively charge above that point. According to the Pb(II) complex speciation diagram, Pb(II) exists dominantly in Pb^{2+} form in acidic to neutral solution and form a solid $Pb(OH)_2$ in basic condition (Powell et al., 2009). The adsorption of Pb(II) onto the surface of adsorbent could follow several possibility, such as complex formation between free surface silanol groups and Pb(II), and formation of anionic complex with Br ion followed by ion-association with phosphonium-cation (Al-bishri et al., 2012; Martinis et al., 2010). The lower efficiency at acidic pH could be due to the competition between hydronium ion and Pb(II) to form complex and the adsorption was mainly done by complex formation with the silanol groups. IL@SIL showed lower adsorption efficiency in low pH solution than that of IL@MSN, which could be associated with the higher presence of silanol groups in the MSN than that of silica (Hamid et al., 2017). Following the pH_{pzc} of the adsorbents, positively charged surface also could contribute in the lower adsorption efficiency at pH below 7, due to electrostatic repulsion between adsorbent and adsorbate. However, the decrease in the adsorption efficiency of both adsorbent in solution with pH above 8 can be associated with the formation of insoluble Pb(II) complexes, such as $Pb(OH)_2$ (Perera et al., 2001). In agreement with N2 physisorption results, the impregnation of $P_{8,8,8,12}Br$ cause a significant impact in the adsorbent porosity, especially in silica, which could be associated with the pore blockage by $P_{8,8,8,12}Br$. This could limit the access of Pb(II) to the additional adsorption sites, which in turn could decrease the adsorption performance.

3.3. *Adsorption kinetic*

The contact time of the experiment was varied from 10 to 120 min to study the adsorption kinetics of both adsorbent. Quantitative adsorption of Pb(II) was achieved by both adsorbent and IL@MSN was able to achieve the quantitative adsorption faster than that of IL@SIL. IL@MSN was able to achieved equilibrium in 60 min, while IL@SIL achieved it in 90 min. Thus, 90 min used in further experiment in this study. Kinetic parameter of the adsorption of Pb(II) by both adsorbent was determined by using the linearized form of pseudo first and pseudo second-order kinetic models, as shown in Eqs. (8) and (9), respectively (Ho and McKay, 1999; Lagergreen, 1907). In addition, the diffusion model of the adsorption process was explored by using the intraparticle diffusion model following the Weber-Morris equation (Eq. (10)) (Qiu et al., 2009).

$$\ln\left(\frac{q_e}{q_e - q_t}\right) = k_1 t \tag{8}$$

$$\frac{1}{(q_e - q_t)} = \frac{1}{q_e} + k_2 t \tag{9}$$

$$q_t = -k_{int} \cdot t^{1/2} \tag{10}$$

where q_{eq} and q_t represents the amount of Pb(II) adsorbed at the equilibrium and at the specified time t. K_1, K_2 and k_{int} are pseudo first-order, pseudo second-order and intraparticle diffusion rate constant, respectively. These parameters were obtained through linear correlation between $log(q_{eq} - q_t)$ and t and between t/q_t and t.

Inferred from the Table 2, adsorption of Pb(II) by both adsorbent fitted nicely with the pseudo second order, which was evidenced by high correlation coefficient (R^2) and the close value between calculated q_{eq} and experimental q_{eq}. It is suggested that adsorption kinetic of Pb(II) controlled by chemical adsorption, which the IL and surface functional groups play an important role (Tran et al., 2020a). Moreover, IL@MSN shows higher rate constant than that of IL@SIL which suggests a faster adsorption of Pb(II) onto IL@MSN than that of IL@SIL. From the interparticle diffusion model, the plot of qt against $t^{1/2}$ yields a finite intercept and this indicates that more than diffusion, boundary layer mechanism could also be involved in following the adsorption kinetics of Pb(II) onto both adsorbents. As the data indicates, diffusion of Pb(II) onto IL@MSN

Table 2 – Isotherm and kinetic parameter for the adsorption of Pb(II).

	Model	Parameters	Value	
			IL@MSN	IL@SIL
Kinetic	Pseudo-first order	K_1	0.0688	0.0413
		$q_{e,exp}$	24.91	24.61
		$q_{e,cal}$	19.73	17.69
		R^2	0.9812	0.9292
	Pseudo-second order	K_2	0.0831	0.0488
		$q_{e,exp}$	24.91	24.61
		$q_{e,cal}$	23.80	24.88
		R^2	0.999	0.998
	Intraparticle diffusion	k_{int}	1.18	1.25
		C	−2.27	−1.21
Isotherms	Langmuir	q_o [mg g^{-1}]	256.4	142.85
		b [L mg^{-1}]	0.042	0.009
		R^2	0.9781	0.8961
		R_L range	0.032-0.32	0.14-0.69
	Freundlich	K_F [$mg^{1-1/n}$ g^{-1} L^{-1}]	25.91	7.30
		n	2.31	2.20
		R^2	0.9981	0.9851
	Temkin	A_T [L mg^{-1}]	1.03	6.94
		b_T [kJ mol^{-1}]	59.82	53.95
		R^2	0.9385	0.9009

is faster than that of IL@SIL, which could be due to the higher porosity of IL@MSN which allows easier access to the adsorption sites.

3.4. Adsorption isotherms

The adsorption of Pb(II) was done at the range of 100–700 mg L^{-1}. Quantitative adsorption of Pb(II) was achieved up until 100 mg L^{-1} and then it was decreasing with the increase of Pb(II) initial concentration which might be due to the saturation of adsorption sites of the adsorbent. The experimental data was then fitted adsorption isotherm models such as Langmuir, Freundlich, and Temkin following the linearized form of the model as presented in the Eqs. (11)–(14), respectively (Dada et al., 2012; Inyinbor et al., 2016):

$$q_e = \frac{Q_o K_L C_e}{1 + K_L C_e} \quad (11)$$

$$Q_e = K_f C_e^{\frac{1}{n}} \quad (12)$$

$$q_e = \frac{RT}{b} \ln(A_T C_e) \quad (13)$$

$$R_L = \frac{1}{(1 + bC_o)} \quad (14)$$

Maximum adsorption capacity was represented by q_o (mg g^{-1}). Langmuir constant was represented by b (L mg^{-1}), which is related to the separation factor (R_L) as shown in Eq. (14). R_L represent the favorability of the adsorption process (R_L = 0: irreversible adsorption; 0 < R_L > 1: favorable adsorption, R_L = 1: linear adsorption, and R_L > 1: unfavorable adsorption). Freundlich adsorption capacity and adsorption heterogeneity were represented by k_F and n, respectively. Temkin equilibrium binding constant and Temkin constant were represented by A_T (L g^{-1}) and b_T (kJ mol L^{-1}). The isotherm parameters were obtained from the linear plot between variation of C_{eq} and q_{eq}.

Table 2 shows the isotherm model parameter for the adsorption of Pb(II). According to the comparison of R^2 values, multilayer adsorption fitted suitably with the sorption of Pb(II) by both IL@SIL and IL@MSN. In addition to excellent adsorption, both adsorbents show high adsorption capacity for Pb(II). However, IL@MSN shows significantly higher capacity than that of IL@SIL, which were 256.4 and 142.85 mg g^{-1}, respectively. High adsorption capacity of IL@MSN could be attributed to the high surface area and porosity. According to the Langmuir model, the separation factor of both metals was between 0 and 1, which suggests adsorption of Pb(II) onto both adsorbents was a favorable process (Tran et al., 2020b). According to Freundlich isotherm model, the n factor values were between 1 and 10, which indicates favorable interaction between adsorbent and adsorbate for both IL@MSN and IL@SIL. Temkin constant (b_T) from the adsorption of both metals were higher than 40 kJ mol^{-1}, which means that the adsorption of Pb(II) with both IL@MSN and IL@SIL was done via a chemisorption process (Ho et al., 2002). Moreover, the isotherms fit in Fig. 6a and b with Langmuir and Freundlich isotherms model shows that the experimental data fitted nicely with Freundlich isotherm models.

3.5. Adsorption thermodynamic

Temperature hold a strong influence and could determine the nature of the reaction. Thus, thermodynamic parameter of Pb(II) adsorption process was investigated at temperature range of 298–328 K. The thermodynamic parameters, such as Gibbs free energy (ΔG, kJ mol^{-1}), enthalpy change (ΔH, kJ mol^{-1}), and entropy change (ΔS, J mol^{-1} K^{-1}) was determined from the experimental data. Those parameters were calculated (given in Table 3) using the linearized Van't Hoff equations, as shown in Eq. (15) (Taka et al., 2018). Moreover, Arrhenius activation energy (E_a, kJ mol^{-1}) of the adsorption process was obtained by using linearized Arrhenius equation, as shown in Eq. (16).

$$\ln K_D = (\Delta S/R) - (\Delta H/RT) \quad (15)$$

$$\ln K_t = \ln (q_{eq}/C_{eq}) = \ln A - (Ea/RT) \quad (16)$$

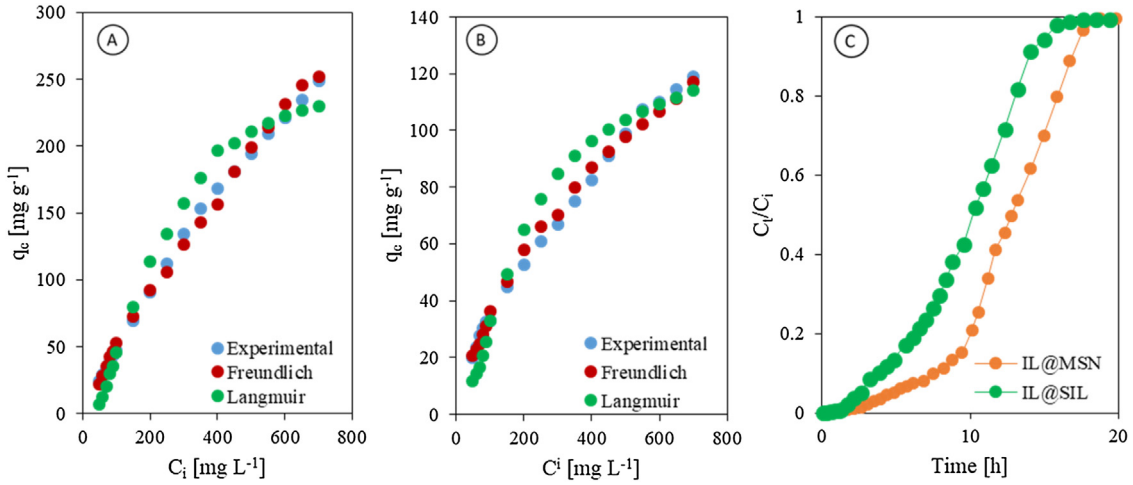

Fig. 6 – Isotherm fit with Langmuir and Freundlich model for (A) IL@MSN and (B)IL@SIL, and (C) breakthrough curve on Pb(II) removal efficiency; [Pb(II)]: 50 mg L^{-1}, adsorbent: 1 g, $P_{8,8,8,12}Br$ loading: 50%, time: 90 min, T: 298 K.

Table 3 – Thermodynamic parameters of the Pb(II) adsorption.

T (K)	IL@MSN			IL@SIL		
	ΔG [kJ mol^{-1}]	ΔH [kJ mol^{-1}]	ΔS [J mol^{-1} K^{-1}]	ΔG [kJ mol^{-1}]	ΔH [kJ mol^{-1}]	ΔS [J mol^{-1} K^{-1}]
298	−70.75	|	|	−23.83	|	|
303	−71.04	|	|	−23.98	|	|
308	−71.61	−53.55	57.68	−24.27	−15.18	29.04
318	−71.90	|	|	−24.42	|	|
328	−72.19	|	|	−24.56	|	|

where R (8.314 J mol^{-1} K^{-1}) and T (K) are the gas constant and temperature. Thermodynamic equilibrium constant (K_D) was obtained from the plot of ln(q_{eq}/C_{eq}) vs C_{eq} at various temperatures (Soetaredjo et al., 2017).

Table 3 shows thermodynamic parameter of the Pb(II) adsorption by both adsorbent. Both adsorptions showed a negative ΔH°, positive ΔS°, and downward trend of ΔG°. These indicates that nature of the process followed exothermic reaction and spontaneous. E_a of Pb(II) adsorption by IL@SIL and IL@MSN were 48.34 and 41.85 kJ mol^{-1}, respectively. The E_a from IL@MSN and IL@SIL were higher than 40 kJ mol^{-1} suggesting that the adsorption follows the chemisorption process (Karmaker et al., 2019). Moreover, IL@MSN results was in agreement with the result from Temkin isotherm model, which presented chemisorption as the main process of Pb(II) adsorption.

3.6. *Column studies*

Table 4 shows the column adsorption parameter for the adsorption Pb(II) by both adsorbents. The increase in bed depth caused increase in the t_{tot} and V_{eff}, which could be due to longer contact time between adsorbate and adsorbent. Increasing trend was also observed in the removal efficiency of Pb(II) due to the increase in the mass of the adsorbent. The q_{eq} of IL@MSN was almost 50% higher than that of IL@SIL, which may be due to the higher surface area and presence of binding sites for the adsorption of Pb(II). Although increase in bed depth provide a positive impact on the column longevity and performance, it is also require a higher number of adsorbent. On the other hand, increased in flow rate followed by a decreased in t_{tot} due to shorter residence time and lower mass resistance of the adsorbent. These factors also negatively affected the removal efficiency of Pb(II). In addition, increased in influent concentration was also found to negatively affect the column exhaustion time. As expected, adsorption capacity increased with increasing influent Pb(II) concentration. This may be caused by faster transport due to higher concentration gradient which increased the mass transfer coefficient. Moreover, q_{tot} and q_{eq} were also increased with an increase in influent Pb(II) concentration. However, IL@MSN showed significantly higher capacity for the adsorption Pb(II) than that of IL@SIL regardless of Pb(II) concentration. This may be attributed to the higher surface properties of IL@MSN, which provide lower mass transfer barrier for the adsorbent. Following the above results, the best conditions for the column adsorption are bed depth of 15 cm, flow rate of 5 mL min^{-1}, and Pb(II) initial concentration of 50 mg L^{-1}. Fig. 6c showed the breakthrough curve on the adsorption of Pb(II) of both IL@MSN and IL@SIL with the best condition for column adsorption. As expected, the column exhaustion time for IL@MSN was significantly longer than that of IL@SIL.

3.6.1. *Model for column adsorption*

Bohart–Adams and Thomas models were used in this study. Bohart–Adams model assume that the equilibrium is not achieved instantaneously and the adsorption rate is influenced proportionally by the residual capacity and metal concentration (Bohart and Adams, 1920). On the other hand, Thomas model was used to evaluate the saturation capacity of the column and the model assumes plug flow behavior in the bed (Thomas, 1944). The linearized equation for Bohart–Adams and Thomas models were presented in the Eqs. (17) and (18) and the result was presented in Table 5 (Chen et al., 2012).

$$\ln(C_t/C_i) = k_{AB} \cdot C_i \cdot t - k_{AB} \cdot N_0 \cdot (Z/U_o) \quad (17)$$

Table 4 – Column adsorption parameter for Pb(II).

C_i	Q	Z	IL@MSN						IL@SIL					
			t_{tot}	m_{tot}	q_{tot}	q_{eq}	V_{eff}	E	t_{tot}	m_{tot}	q_{tot}	q_{eq}	V_{eff}	E
50	5	10	1060	265	248	83	5300	94	900	225	157	52	4500	70
50	5	15	1240	310	288	58	6200	93	677	169	129	26	3385	76
50	5	20	1420	355	338	48	7100	95	401	100	80	11	2005	80
50	5	10	1060	265	248	83	5300	94	900	225	157	52	4500	70
50	10	10	850	425	358	119	8500	84	521	261	157	52	5210	60
50	15	10	640	480	376	125	9600	78	379	284	154	51	5685	54
50	5	10	1060	265	248	83	5300	94	900	225	157	52	4500	70
100	5	10	710	355	306	102	3550	86	608	304	183	61	3040	60
200	5	10	590	590	467	156	2950	79	368	368	203	68	1840	55

C_i = mg L^{-1}; Q = mL min^{-1}; Z = cm; t_{tot} = min; m_{tot} = mg; q_{tot} = mg; q_{eq} = mg g^{-1}; E = %.

Table 5 – Parameter for column adsorption model.

IL@MSN			Bohart–Adams model			Thomas model		
Ci	Q	Z	k_{AB} ($\times 10^{-3}$)	N_0	R^2	k_{TH} ($\times 10^{-2}$)	q_e	R^2
50	5	10	6.9	129.2	0.882	1.23	325.6	0.982
50	5	15	4.1	105.1	0.721	0.72	207.1	0.935
50	5	20	2.6	91.6	0.766	0.55	173.2	0.953
50	5	10	6.9	129.2	0.882	1.23	325.6	0.982
50	10	10	4.3	98.5	0.691	1.98	257.5	0.951
50	15	10	2.2	70.9	0.801	2.32	195.3	0.967
50	5	10	6.9	129.2	0.882	1.23	325.6	0.982
100	5	10	3.4	95.1	0.747	1.05	265.4	0.970
200	5	10	1.6	69.9	0.635	0.77	220.5	0.961
IL@SIL								
50	5	10	6.7	113.4	0.740	1.15	242.2	0.945

Table 6 – Comparison of sorption capacities of various immobilized IL on solid support.

Adsorbent	System	Analyte	Adsorption capacity [mg g^{-1}]	Ref.
Aliquat 336/SBA-15	Batch adsorption	Pd(II)	212.76	Sharma et al. (2016)
Aliquat 336/chitosan		Pd(II)	187.61	Kumar et al. (2015b)
C_4mim Tf_2N/nanosilica		Pb(II)	267.03	Al-bishri et al. (2012)
C_{16}mim Cl/montmorillonite		Dye	263.2	Lawal and Moodley (2015)
PyCl/Pluronic F127		Pb(II)	202.3	Wieszczycka et al. (2021)
MSN		Pb(II)	182.44	Present work
Silica		Pb(II)	101.07	Present work
$P_{8,8,8,12}$Br/MSN		Pb(II)	256.40	Present work
$P_{8,8,8,12}$Br/silica		Pb(II)	142.85	Present work
Aminopropylmim NO_3/cellulose	Column adsorption	Cr(VI)	113.5	Dong and Zhao (2018)
Heptylammonium Br/MWCNT		Cr(VI)	85.83	Kumar et al. (2015a)
Imidazole HSO_4/silica		Pb(II)	139.28	Song et al. (2016)
C_{16}mim Cl/*Kigelia Pinnata*		Drug	73	Lawal and Moodley (2017)
$P_{8,8,8,12Br}$/MSN		Pb(II)	325.60	Present work
$P_{8,8,8,12Br}$/silica		Pb(II)	242.20	Present work

$$\ln(C_t/C_i - 1) = k_{TH} \cdot q_e \cdot (m/Q) - k_{TH} \cdot C_i \cdot t \quad (18)$$

where C_i and C_t are the influent and effluent concentration (mg L^{-1}), respectively, Z is the bed depth of the fix-bed column (cm) and U_0 is the superficial velocity (cm min^{-1}) defined as the ratio of the volumetric flow rate (Q, cm^3 min^{-1}) to the cross-sectional area of the bed (A, cm^2) and m is the amount of adsorbent in the column. k_{AB} (L mg^{-1} min^{-1}) and N_0 (mg L^{-1}) represent the solute uptake rate and saturation concentration, respectively, which were obtainable from the linear plot between $\ln(C_t/C_i)$ against t. In addition, k_{TH} (L mg^{-1} min^{-1}) and q_e (mg L^{-1}) represent the Thomas rate constant and saturation loading capacity, which were obtainable from the linear plot between $\ln((C_t/C_i) - 1)$ against t.

The respective values of the models parameter for IL@MSN and IL@SIL were presented in Table 5. As shown in Table 5, IL@MSN showed higher uptake rate and saturation concentration than that of IL@SIL. This could be due to the superior surface properties of IL@MSN which allows faster diffusion of the solute (López-Cervantes et al., 2018). The values of k_{AB} decreased with increase of flow rate, bed depth and influent Pb(II) concentration. It could be inferred that the system kinetics was strongly influence by external mass transfer in the initial part of adsorption in the column (Sharma and Singh, 2013). However, the low R^2 value indicates that the model was not suitable as a predictor for the breakthrough curve. In agreement with Bohart–Adams model, IL@MSN showed higher rate constant and saturation loading capac-

ity in Thomas model than that of IL@SIL. From Table 5, it can be seen that k_{TH} value was decreased with the increase in bed depth and influent Pb(II) concentration. The decrease of k_{TH} due to influent Pb(II) concentration was attributed to higher concentration difference as driving force for adsorption. However, k_{TH} values increased with the increase in flow rate, while the value of q_e decreased. This could be caused by the decrease in contact time between adsorbate and the column and hence Pb(II) ions do not have enough time to bind with the column active sites or diffuse into the pores (Sharma et al., 2016). Results indicate that lowest metal concentration in feed, adsorbent bed height, and high feed flow rate is favorable for higher adsorption of Pb(II). Moreover, the R^2 values showed suitability of Thomas model for adsorption of Pb(II) using both IL@MSN and IL@SIL.

3.7. *Comparison with other adsorbents*

The comparison of adsorption efficiency of Pb(II) using immobilized IL was presented in Table 6. The performance of IL@MSN and IL@SIL was also compared with the native materials. As shown in Table 6, the immobilization of $P_{8,8,8,12}Br$ onto MSN and silica significantly enhanced the adsorption capacity of both materials than that of native MSN and silica. The surface silanol groups within the native MSN and silica could act as the adsorption sites for Pb(II) and the additional adsorption capacity of IL@MSN and IL@SIL could be associated with the presence of $P_{8,8,8,12}Br$. Moreover, adsorption performance of IL@MSN is higher than many other adsorbents, in both batch and column adsorption process. It shows that the potential of IL@MSN for removal of heavy metal from aqueous solution.

4. Conclusions

Silica-based materials was successfully impregnated with a phosphonium-based ionic liquid. The adsorbent was successfully used for Pb(II) removal from aqueous solution. IL@MSN showed better performance than that of IL@SIL, in terms of kinetic, thermodynamic and reusability. IL@MSN was able to remove more than 90% of Pb(II) from aqueous solution within 90 min. The adsorption of Pb(II) by both adsorbents followed multilayer adsorption pathway as the isotherms data were best fitted with the Freundlich isotherm model. Moreover, pseudo-second order kinetic model was best fitted with the kinetic data by both adsorbents. From thermodynamic studies, the adsorption process was spontaneous, exothermic in nature and follow chemisorption pathway for IL@MSN. The breakthrough curves of both adsorbent were reasonably fitted using Thomas model with a high adsorption capacity of 325.6 and 242.2 mg g^{-1} for IL@MSN and IL@SIL, respectively. The optimum sorption capacity was obtained at flow rate of 5 mL min^{-1} and bed height of 10 cm as the highest Pb(II) removal efficiency was achieved at 94 and 70% for IL@MSN and IL@SIL, respectively. From the above results, it could be concluded IL impregnated silica-based materials have potential as adsorbent for heavy metals and mesoporous silica nanaparticles with higher surface area and porosity could provide faster kinetic and more favorable reaction thermodynamic than its counterpart.

Conflict of interests

The authors declare that they have no conflict of interest.

Funding

This work was supported by the Universitas Airlangga under Hibah Riset Mandat grant [grant numbers 395/UN3.14/PT/2020].

CRediT authorship contribution statement

Mochamad L. Firmansyah: Conceptualization, Methodology, Investigation, Writing – original draft, Visualization, Funding acquisition. **Nurul S. Hassan:** Methodology, Investigation. **Aishah A. Jalil:** Writing – review & editing, Resources. **Rino R. Mukti:** Writing – review & editing, Supervision, Resources. **Teh L. Peng:** Writing – review & editing, Supervision. **Herma D. Setiabudi:** Writing – review & editing, Resources.

Acknowledgements

This work was supported by Universitas Airlangga under grant Hibah Riset Mandat 2020. The authors are gratefully acknowledging to the Universiti Teknologi Malaysia for the Professional Development Research University Grant (No. 05E44). The authors are grateful towards Central Laboratory of Universitas Islam Indonesia, Yogyakarta for the assistance in the adsorbent characterization.

References

Al-bishri, H.M., Abdel-Fattah, T.M., Mahmoud, M.E., 2012. Immobilization of [Bmim+Tf 2N−] hydrophobic ionic liquid on nano-silica-amine sorbent for implementation in solid phase extraction and removal of lead. J. Ind. Eng. Chem. 18, 1252–1257, http://dx.doi.org/10.1016/j.jiec.2012.01.018.

Ali, H., Khan, E., Ilahi, I., 2019. Environmental chemistry and ecotoxicology of hazardous heavy metals: environmental persistence, toxicity, and bioaccumulation. J. Chem. 2019, http://dx.doi.org/10.1155/2019/6730305.

Ayata, S., Bozkurt, S.S., Ocakoglu, K., 2011. Separation and preconcentration of Pb(II) using ionic liquid-modified silica and its determination by flame atomic absorption spectrometry. Talanta 84, 212–215, http://dx.doi.org/10.1016/j.talanta.2011.01.006.

Aziz, M.A.A., Jalil, A.A., Triwahyono, S., Mukti, R.R., Taufiq-Yap, Y.H., Sazegar, M.R., 2014. Highly active Ni-promoted mesostructured silica nanoparticles for CO_2 methanation. Appl. Catal. B Environ. 147, 359–368, http://dx.doi.org/10.1016/j.apcatb.2013.09.015.

Bandehali, S., Parvizian, F., Moghadassi, A.R., Hosseini, S.M., Shen, J.N., 2020. Fabrication of thin film-PEI nanofiltration membrane with promoted separation performances: Cr, Pb and Cu ions removal from water. J. Polym. Res. 27, http://dx.doi.org/10.1007/s10965-020-02056-x.

Bohart, G.S., Adams, E.Q., 1920. Some aspects of the behavior of charcoal with respect to chlorine. J. Franklin Inst. 189, 669, http://dx.doi.org/10.1016/s0016-0032(20)90400-3.

Bradaric, C.J., Downard, A., Kennedy, C., Robertson, A.J., Zhou, Y., 2003. Industrial preparation of phosphonium ionic liquids Portions of this work were presented at the following meetings: (a) 224th American Chemical Society Conference, Boston, USA, 2002; (b) Green Solvents for Catalysis Meeting, held in Bruchsal, Germany, 13–16th October 2002. Green Chem. 5, 143–152, http://dx.doi.org/10.1039/b209734f.

Bukhari, S.N., Chong, C.C., Setiabudi, H.D., Cheng, Y.W., Teh, L.P., Jalil, A.A., 2021. Ni/Fibrous type SBA-15: highly active and coke resistant catalyst for CO_2 methanation. Chem. Eng. Sci. 229, 116141, http://dx.doi.org/10.1016/j.ces.2020.116141.

Chen, S., Yue, Q., Gao, B., Li, Q., Xu, X., Fu, K., 2012. Bioresource Technology Adsorption of hexavalent chromium from

aqueous solution by modified corn stalk: a fixed-bed column study. Bioresour. Technol. 113, 114–120, http://dx.doi.org/10.1016/j.biortech.2011.11.110.
Da'na, E., 2017. Adsorption of heavy metals on functionalized-mesoporous silica: a review. Microporous Mesoporous Mater. 247, 145–157, http://dx.doi.org/10.1016/j.micromeso.2017.03.050.
Dada, A., Olalekan, A., Olatunya, A., Dada, O., 2012. Langmuir, Freundlich, Temkin and Dubinin–Radushkevich isotherms studies of equilibrium sorption of Zn^{2+} unto phosphoric acid modified rice husk. IOSR J. Appl. Chem. 3, 38–45, http://dx.doi.org/10.9790/5736-0313845.
Dharaskar, S.A., Wasewar, K.L., Varma, M.N., Shende, D.Z., Tadi, K.K., Yoo, C.K., 2014. Synthesis, characterization, and application of novel trihexyl tetradecyl phosphonium bis (2,4,4-trimethylpentyl) phosphinate for extractive desulfurization of liquid fuel. Fuel Process. Technol. 123, 1–10, http://dx.doi.org/10.1016/j.fuproc.2014.02.001.
Dong, Z., Zhao, L., 2018. Covalently bonded ionic liquid onto cellulose for fast adsorption and efficient separation of Cr(VI): batch, column and mechanism investigation. Carbohydr. Polym. 189, 190–197, http://dx.doi.org/10.1016/j.carbpol.2018.02.038.
Firmansyah, M.L., Fajar, A.T.N., Yoshida, W., Hanada, T., Goto, M., 2020. Liquid–Liquid extraction of Cd(II) and Zn(II) using a novel tetraalkylphosphonium-based ionic liquid. J. Chem. Eng. Jpn. 53, 1–8, http://dx.doi.org/10.1252/jcej.20we030.
Goyal, P., Tiwary, C.S., Misra, S.K., 2021. Ion exchange based approach for rapid and selective Pb(II) removal using iron oxide decorated metal organic framework hybrid. J. Environ. Manage. 277, 111469, http://dx.doi.org/10.1016/j.jenvman.2020.111469.
Halli, P., Agarwal, V., Partinen, J., Lundström, M., 2020. Recovery of Pb and Zn from a citrate leach liquor of a roasted EAF dust using precipitation and solvent extraction. Sep. Purif. Technol. 236, 116264, http://dx.doi.org/10.1016/j.seppur.2019.116264.
Hamid, M.Y.S., Firmansyah, M.L., Triwahyono, S., Jalil, A.A., Mukti, R.R., Febriyanti, E., Suendo, V., Setiabudi, H.D., Mohamed, M., Nabgan, W., 2017. Oxygen vacancy-rich mesoporous silica KCC-1 for CO_2 methanation. Appl. Catal. A Gen. 532, 86–94, http://dx.doi.org/10.1016/j.apcata.2016.12.023.
Ho, Y., McKay, G., 1999. Pseudo-second order model for sorption processes. Process Biochem. 34, 451–465, http://dx.doi.org/10.1016/S0032-9592(98)00112-5.
Ho, Y.S., Porter, J.F., Mckay, G., 2002. Divalent metal ions onto peat: copper, nickel and lead single component systems. Water Air Soil Pollut. 141, 1–33.
Huynh, J., Palacio, R., Allavena, A., Gallard, H., Descostes, M., Mamède, A., Royer, S., Tertre, E., Batonneau-gener, I., 2021. Selective adsorption of U(VI) from real mine water using an NH2-functionalized silica packed column. Chem. Eng. J. 405, 126912, http://dx.doi.org/10.1016/j.cej.2020.126912.
Inyinbor, A.A., Adekola, F.A., Olatunji, G.A., 2016. Kinetics, isotherms and thermodynamic modeling of liquid phase adsorption of Rhodamine B dye onto *Raphia hookerie* fruit epicarp. Water Resour. Ind. 15, 14–27, http://dx.doi.org/10.1016/j.wri.2016.06.001.
Jumina, Priastomo, Y., Setiawan, H.R., Mutmainah, Kurniawan, Y.S., Ohto, K., 2020. Simultaneous removal of lead(II), chromium(III), and copper(II) heavy metal ions through an adsorption process using C-phenylcalix[4]pyrogallolarene material. J. Environ. Chem. Eng. 8, 103971, http://dx.doi.org/10.1016/j.jece.2020.103971.
Karmaker, S., Sintaha, F., Saha, T.K., 2019. Kinetics, isotherm and thermodynamic studies of the adsorption of reactive red 239 dye from aqueous solution by chitosan 8B. Adv. Biol. Chem. 09, 1–22, http://dx.doi.org/10.4236/abc.2019.91001.
Kumar, A. Santhana Krishna, Jiang, S., Tseng, W., 2015a. Effective adsorption of chromium(vi)/Cr(iii) from aqueous solution using ionic liquid functionalized multiwalled carbon nanotubes as a super sorbent. J. Mater. Chem. A 3, 7044–7057, http://dx.doi.org/10.1039/C4TA06948J.
Kumar, A. Santhana Krishna, Sharma, S., Reddy, R.S., Barathi, M., Rajesh, N., 2015b. Comprehending the interaction between chitosan and ionic liquid for the adsorption of palladium. Int. J. Biol. Macromol. 72, 633–639, http://dx.doi.org/10.1016/j.ijbiomac.2014.09.002.
Lagergreen, S., 1907. Zur Theorie der sogenannten Adsorption gelöster Stoffe. Zeitschrift für Chemie und Ind. der Kolloide 2, 174–175, http://dx.doi.org/10.1007/BF01501332.
Lawal, I.A., Moodley, B., 2017. Sorption mechansim of pharmaceuticals from aqueous medium on ionic liquid modified biomass. J. Chem. Technol. Biotechnol. 92, 808–818, http://dx.doi.org/10.1002/jctb.5063.
Lawal, I.A., Moodley, B., 2015. Synthesis, characterisation and application of imidazolium based ionic liquid modified montmorillonite sorbents for the removal of amaranth dye. RSC Adv. 5, 61913–61924, http://dx.doi.org/10.1039/c5ra09483f.
López-Cervantes, J., Sánchez-Machado, D.I., Sánchez-Duarte, R.G., Correa-Murrieta, M.A., 2018. Study of a fixed-bed column in the adsorption of an azo dye from an aqueous medium using a chitosan–glutaraldehyde biosorbent. Adsorpt. Sci. Technol. 36, 215–232, http://dx.doi.org/10.1177/0263617416688021.
Martinis, E.M., Bertón, P., Altamirano, J.C., Hakala, U., Wuilloud, R.G., 2010. Tetradecyl(trihexyl)phosphonium chloride ionic liquid single-drop microextraction for electrothermal atomic absorption spectrometric determination of lead in water samples. Talanta 80, 2034–2040, http://dx.doi.org/10.1016/j.talanta.2009.11.012.
Ministry of Environment and Forestry of The Republic of Indonesia, 2014. Peraturan Menteri Lingkungan Hidup RI No. 5 Tahun 2014 Tentang Baku Mutu Air Limbah. Kementrian Lingkungan Hidup dan Kehutanan.
Mohamed, W.R., Metwally, S.S., Ibrahim, H.A., El-Sherief, E.A., Mekhamer, H.S., Moustafa, I.M.I., Mabrouk, E.M., 2017. Impregnation of task-specific ionic liquid into a solid support for removal of neodymium and gadolinium ions from aqueous solution. J. Mol. Liq. 236, 9–17, http://dx.doi.org/10.1016/j.molliq.2017.04.013.
Nasir, M.S.R.M., Khairunnisa, M.P., Jusoh, N.W.C., Jalil, A.A., 2020. Enhanced carbon dioxide adsorption by amine-modified KCC-1. IOP Conf. Ser. Earth Environ. Sci. 476, http://dx.doi.org/10.1088/1755-1315/476/1/012084.
Palupi, E.S., Sulistyarti, H., Abdjan, M.I., Anjasmara, C., Putra, R., 2020. Studi aktivitas ditizon sebagai pengompleks ion Pb2+ menggunakan metode spektrofotometri UV-vis dan semi empiris AM1. Jurnal Muara 4, 423–432.
Perera, W.N., Hefter, G., Sipos, P.M., 2001. An investigation of the Lead(II)-hydroxide system. Inorg. Chem. 40, 3974–3978.
Powell, K.J., Brown, P.L., Byrne, R.H., Gajda, T., Hefter, G., Leuz, A.K., Sjöberg, S., Wanner, H., 2009. Chemical speciation of environmentally significant metals with inorganic ligands. Part 3: the Pb^{2+} + OH^-, Cl^-, CO_3^{2-}, SO_4^{2-}, and PO_4^{3-} systems (IUPAC Technical Report). Pure Appl. Chem. 81, 2425–2476, http://dx.doi.org/10.1351/PAC-REP-09-03-05.
Qiu, H., Lv, L., Pan, B.C., Zhang, Q.J., Zhang, W.M., Zhang, Q.X., 2009. Critical review in adsorption kinetic models. J. Zhejiang Univ. Sci. A 10, 716–724, http://dx.doi.org/10.1631/jzus.A0820524.
Rameli, N., Jumbri, K., Wahab, R.A., Ramli, A., Huyop, F., 2018. Synthesis and characterization of mesoporous silica nanoparticles using ionic liquids as a template. J. Phys. Conf. Ser. 1123, http://dx.doi.org/10.1088/1742-6596/1123/1/012068.
Sankhla, M.S., Kumari, M., Nandan, M., Kumar, R., Agrawal, P., 2019. Heavy metals contamination in water and their hazardous effect on human health—a review. SSRN Electron. J. 5, 759–766, http://dx.doi.org/10.2139/ssrn.3428216.
Shahbazi, A., Younesi, H., Badiei, A., 2012. Batch and fixed-bed column adsorption of Cu(II), Pb(II) and Cd(II) from aqueous solution onto functionalised SBA-15 mesoporous silica. Can. J. Chem. Eng. 91, 739–750, http://dx.doi.org/10.1002/cjce.21691.
Sharma, G., Kumar, A., Naushad, M., Thakur, B., Vo, D.N., Gao, B., Al-kahtani, A.A., Stadler, F.J., 2021. Adsorptional-photocatalytic removal of fast sulphon black dye by using chitin-cl-poly (itaconic

acid-co-acrylamide)/zirconium tungstate nanocomposite hydrogel. J. Hazard. Mater. 416, 125714, http://dx.doi.org/10.1016/j.jhazmat.2021.125714.
Sharma, G., Thakur, B., Kumar, A., Sharma, S., Naushad, M., Stadler, F.J., 2020. Atrazine removal using chitin-cl-poly (acrylamide-co-itaconic acid) nanohydrogel: Isotherms and pH responsive nature. Carbohydr. Polym. 241, 116258, http://dx.doi.org/10.1016/j.carbpol.2020.116258.
Sharma, R., Singh, B., 2013. Removal of Ni(II) ions from aqueous solutions using modified rice straw in a fixed bed column. Bioresour. Technol. 146, 519–524, http://dx.doi.org/10.1016/j.biortech.2013.07.146.
Sharma, S., Wu, C.M., Koodali, R.T., Rajesh, N., 2016. An ionic liquid-mesoporous silica blend as a novel adsorbent for the adsorption and recovery of palladium ions, and its applications in continuous flow study and as an industrial catalyst. RSC Adv. 6, 26668–26678, http://dx.doi.org/10.1039/c5ra26673d.
Soetaredjo, F.E., Ju, Y.H., Ismadji, S., Ayucitra, A., 2017. Removal of cu(II) and pb(II) from wastewater using biochar-clay nanocomposite. Desalin. Water Treat. 82, 188–200, http://dx.doi.org/10.5004/dwt.2017.20969.
Song, H., Yang, C., Yohannes, A., Yao, S., 2016. Acidic ionic liquid modified silica gel for adsorption and separation of bovine serum albumin (BSA). RSC Adv. 6, 107452–107462, http://dx.doi.org/10.1039/c6ra23372d.
Taka, A.L., Fosso-Kankeu, E., Pillay, K., Mbianda, X.Y., 2018. Removal of cobalt and lead ions from wastewater samples using an insoluble nanosponge biopolymer composite: adsorption isotherm, kinetic, thermodynamic, and regeneration studies. Environ. Sci. Pollut. Res. 25, 21752–21767, http://dx.doi.org/10.1007/s11356-018-2055-6.
Thomas, H.C., 1944. Heterogeneous ion exchange in a flowing system. J. Am. Chem. Soc. 66, 1664–1666, http://dx.doi.org/10.1021/ja01238a017.
Tran, T. Van, Nguyen, D.T.C., Nguyen, T.T., Le, H.T.N., Nguyen, C. Van, Nguyen, T.D., 2020a. Metal-organic framework HKUST-1-based Cu/Cu_2O/CuO@C porous composite: rapid synthesis and uptake application in antibiotics remediation. J. Water Process Eng. 36, 101319, http://dx.doi.org/10.1016/j.jwpe.2020.101319.
Tran, T. Van, Phan, T.Q.T., Nguyen, D.T.C., Nguyen, T.T., Nguyen, D.H., Vo, D.V.N., Bach, L.G., Nguyen, T.D., 2020b. Recyclable Fe_3O_4@C nanocomposite as potential adsorbent for a wide range of organic dyes and simulated hospital effluents. Environ. Technol. Innov. 20, 101122, http://dx.doi.org/10.1016/j.eti.2020.101122.
Triwahyono, S., Salamun, N., Jalil, A.A., Izan, S.M., Setiabudi, H.D., Prasetyoko, D., 2019. Zirconium-loaded mesostructured silica nanoparticles adsorbent for removal of hexavalent chromium from aqueous solution. Ind. Eng. Chem. Res. 58, 704–712, http://dx.doi.org/10.1021/acs.iecr.8b02167.
Ullah, Z., Azmi Bustam, M., Man, Z., Khan, A.S., 2016. Phosphonium-based ionic liquids and their application in separation of dye from aqueous solution. ARPN J. Eng. Appl. Sci. 11, 1653–1659.
Wieszczycka, K., Filipowiak, K., Wojciechowska, I., Buchwald, T., Siwińska-Ciesielczyk, K., Strzemiecka, B., Jesionowski, T., Voelkel, A., 2021. Novel highly efficient ionic liquid-functionalized silica for toxic metals removal. Sep. Purif. Technol. 265, http://dx.doi.org/10.1016/j.seppur.2021.118483.